

Optimized voltage injection techniques for protection of sensitive loads

J.R.S. Martins^a, D.A. Fernandes^b, F.F. Costa^c, M.B.R. Corrêa^d, A.J. Sguarezi Filho^e,
E.R.C. da Silva^b

^a Federal University of Alagoas, Maceió, AL, Brazil

^b Federal University of Paraíba, João Pessoa, PB, Brazil

^c Federal University of Bahia, Salvador, BA, Brazil

^d Federal University of Campina Grande, Campina Grande, PB, Brazil

^e Federal University do ABC, Santo André, SP, Brazil

ARTICLE INFO

Keywords:

Dynamic voltage restorer

Multi-resonant control

Power injection

Series compensation

Voltage sag

ABSTRACT

This paper proposes voltage compensation method performed by a dynamic voltage restorer (DVR) that minimizes its output power and can also be adapted to minimize its compensating voltage amplitude. The method relies on the construction of a proper voltage reference which takes into account the load power factor and makes use of a recursive least square (RLS) technique. The RLS estimates the grid voltage amplitude and can also be applied to estimate the grid voltage phase, in the case of the minimization of the injected voltage amplitude. This paper also introduces a repetitive controller to track the compensating voltage. This controller is suitable for sinusoidal references and is robust to harmonic distortions, sags and swells. Simulated and experimental results show the DVR efficacy to protect the load under different deviations of the grid voltage.

1. Introduction

Nowadays, due to the increasing number of nonlinear loads connected to the power grid, the presence of harmonic voltages in the distribution level is a matter of great concern. In addition, it is reported that sags and swells are among the most common power quality (PQ) problem inflicting the utility's customers [1]. Furthermore, the portion of sensitive and critical loads, based on power electronics, connected to the grid are significant [2,3]. This scenario suggests the importance of multi-focused PQ solutions.

With regards to grid faults, two types of approaches are described to deal with such problems. The first one is to increase the capacity of the power grid in coping with the effects of the faults by means of actions that lead to the redundancy of the power supply, refinement of maintenance procedures or replacement of obsolete or aged equipment [4–6]. These actions are based on overall vision of the grid and usually are taken by utilities, which are central agents for the system. The other approach is complementary to the first one and seeks for local solutions, usually implanted by the utilities' costumers. This latter approach is typified by the usage of equipment such as DVRs or series power filters [1,7–9].

Numerous problems that inflict critical loads and negatively score the quality of the power grid are the short-duration voltage variations,

represented in greater numbers by voltage sags and swells [10–13]. Dynamic voltage restorers and uninterrupted power supplies are the appliances that best represent custom power devices for repairing these disturbances [14–16]. In addition to sags and swells, harmonic distortions are disturbances commonly presented in the grid voltages. Therefore, there is a clear demand for devices capable of dealing with different kinds of variations. The DVR proposed in this paper is aimed to this purpose.

A compensating voltage from a DVR can be constructed in three different forms. In the first one, the voltage level is minimum. The second form is executed to assure that the DVR output power is null or minimum. In the third one, the compensating voltage is built to establish the pre-sagged voltage conditions [17]. This latter form has the drawback of not allowing the optimization of both power and voltage level. Voltage levels are optimized in [14,16,18,19]. In [3,20], the DVR control systems operate to minimize the power injected from the DVR into the grid. The voltage restoration to pre-sagged conditions are proposed in [3,8,21,22].

A method that minimizes the DVR output power is introduced in this paper. The method consists of the generation of a proper voltage reference to the DVR controller. This reference assures that the output power is null or minimum. It is built with the assistance of an RLS algorithm [23,24] that computes the grid voltage amplitude. The phase

E-mail addresses: joao@ic.ufal.br (J.R.S. Martins), darlan@cear.ufpb.br (D.A. Fernandes), fabiano.costa@ufba.br (F.F. Costa), mbrcorrea@dee.ufcg.edu.br (M.B.R. Corrêa), alfeu.sguarezi@ufabc.edu.br (A.J. Sguarezi Filho), edison.roberto@cear.ufpb.br (E.R.C. da Silva).

<https://doi.org/10.1016/j.ijepes.2019.105569>

Received 19 April 2019; Received in revised form 8 August 2019; Accepted 23 September 2019

0142-0615/ © 2019 Elsevier Ltd. All rights reserved.

for the reference is determined by a reasoning which takes into account the power factor of the load covered by the DVR.

In addition to the voltage reference construction, this paper also proposes a repetitive controller which rules the compensating voltages in each phase separately [25]. This control strategy advantages over dq control schemes [19,26] that usually requires estimation of the positive sequence component of the three-phase voltages [27]. In addition, this kind of control can promptly be applied to single-phase systems. The repetitive control is suitable as it is a resonant controller which tracks sinusoidal references [28–30]. But unlike this latter controller, it is represented by a simple transcendental transfer function equivalent to infinite resonant controllers in parallel. This avoids the need of multiples selective harmonic filters which would increase the computational complexity of the system [31,32]. It is worth mentioning that another alternative to track sinusoidal references is suggested in [33], based in a fractional order proportional integral.

Finally, it is important to point out that the voltage reference generation procedure proposed in this paper can easily be adapted to also minimize the voltage amplitude injected by the DVR. This is due to the fact that the RLS algorithm also can be applied to estimate the phase of the grid voltage beyond its amplitude. This possibility is exploit in this paper and results are produced using such approach.

2. Process and control system design

Fig. 1(a) presents the proposal of the series compensator in which the single-phase equivalent is shown in Fig. 1(b).

This way, v_{pcc} is the voltage applied on the point of common coupling (PCC). The current i_s from the power grid has two components: i_r due to the all the other loads connected to the same bus and the current i that supplies the critical load, L and R are the inductance and the resistance related to the series coupling transform of the compensator, v is the voltage applied to the sensitive load and u is the adjusting voltage.

The sensitive load voltage can be represented by:

$$v(t) = v_{pcc}(t) - Ri(t) - L \frac{d}{dt}i(t) + u(t). \quad (1)$$

The control proposal of this paper employing (1) is depicted

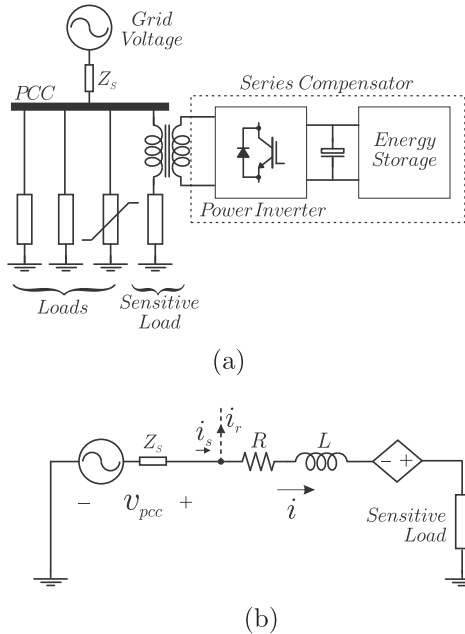


Fig. 1. Protected sensitive load. (a) Single-ended electrical representation for disturbance compensation. (b) Grid compensation and load in single-phase representation.

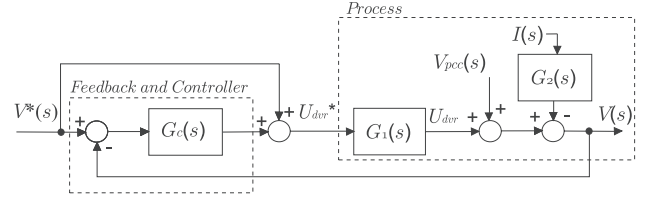


Fig. 2. Repetitive control scheme for the series compensator.

according to the diagram block shown in Fig. 2.

The transfer functions G_1 and G_2 represent the system to be controlled. Due to high switching frequency the dynamic voltage restore can be modeled as delay $G_1 = e^{-t_0s}$ in which it is the sum of a sampling and switching periods. The transfer function $G_2 = Ls + R$ represents the impedance of the coupling transformer, and G_c is the repetitive controller of the system. The entries of the control system are the reference voltage to be applicable on the critical load (V^*), the common coupling voltage V_{pcc} and the current I from the grid. And, U_{dvr}^* is the voltage produced by the proposed DVR control system. Thus, it can be rewrite as:

$$V(s) = F_r(s)V^*(s) + F_g(s)V_{pcc}(s) + F_i(s)I(s), \quad (2)$$

where

$$F_r(s) = \frac{[1 + G_c(s)]G_1(s)}{1 + G_c(s)G_1(s)}, \quad (3)$$

$$F_g(s) = \frac{1 - G_1(s)}{1 + G_c(s)G_1(s)}, \quad (4)$$

$$F_i(s) = -\frac{G_2(s)}{1 + G_c(s)G_1(s)}. \quad (5)$$

In the repetitive control theory [34], the controller, as a rule, can be written as:

$$G_c(s) = \frac{Q(s)}{1 - e^{-\frac{2\pi}{\omega_1}s}}, \quad (6)$$

where ω_1 is the grid frequency and $Q(s)$ is the transfer function that guarantees the feedback system stability. Substituting (6) in (3)–(5) carry out

$$F_r(s) = \frac{[1 - e^{-\frac{2\pi}{\omega_1}s} + Q(s)]G_1(s)}{1 - e^{-\frac{2\pi}{\omega_1}s} + Q(s)G_1(s)}, \quad (7)$$

$$F_g(s) = \frac{[1 - G_1(s)][1 - e^{-\frac{2\pi}{\omega_1}s}]}{1 - e^{-\frac{2\pi}{\omega_1}s} + Q(s)G_1(s)}, \quad (8)$$

$$F_i(s) = -\frac{[1 - e^{-\frac{2\pi}{\omega_1}s}]G_2}{1 - e^{-\frac{2\pi}{\omega_1}s} + Q(s)G_1(s)}. \quad (9)$$

When the frequency response of (7)–(9) is examined the terms $(1 - e^{-\frac{2\pi}{\omega_1}j\omega})$ are zero when ω is a multiple of ω_1 , with $s = j\omega$. This way, $F_g(j\omega_h) = 0$, $F_i(j\omega_h) = 0$ and $F_r(j\omega_h) = 1$, in case of $\omega_h = h\omega_1$, where $h = 0, 1, 2, \dots, \infty$. Thus, by analyzing (2), the voltage V produced by the output of the control system is the reference voltage V^* . This is a guarantee that the output tracks the reference.

The system can be unstable if $Q(s) = e^{-\frac{2\pi}{\omega_1}Ts}$ [35]. Hence, it is possible to make changes in $G_c(s)$ and it becomes

$$G_c(s) = \frac{F(s)e^{-(T-\hat{t}_0)s}}{1 - F(s)e^{-Ts}}, \quad (10)$$

where \hat{t}_0 is the estimated time delay for the DVR, $F(s)$ is a low-pass filter transfer function, T is the fundamental period minus δ . This parameter is chosen by means $\delta < (2\pi/\omega_1)$. This way, the alteration in

Table 1
Parameters designed to the control system.

Parameter	Value
δ	555 μ s
f_s	10 kHz
\hat{t}_0	$1/(2f_s)$
T	16.11 ms
ω_1	377 rad/s

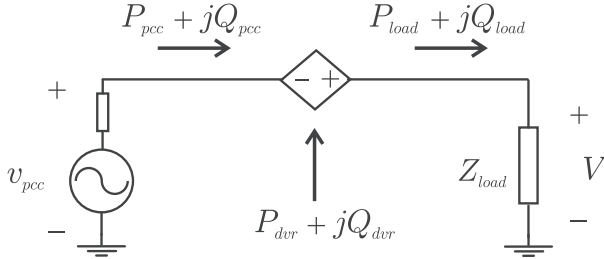


Fig. 3. References of power flow directions.

the equation of the controller guarantees reproduction of the references and the harmonic mitigation. The parameters used in this proposed system are summarized in Table 1.

3. Strategies of voltage sag compensation

Fig. 3 is a schematic representation of the power grid supplying a load that is protected by a DVR. It is depicted in this figure, the complex power flowing through the whole system. The voltage U_{dvr} can be generated by the DVR in three modes which are illustrated in Fig. 4. In the first mode, the applied voltage on the load has the same phase-angle of the pre-dipped grid voltage. This case has the advantage to avoid phase-jumps which can be destructive to sensitive loads. The second operation mode occurs when the voltage correction is performed by applying voltage synchronously during the voltage sag. This scheme requires lower levels of voltages and it is very interesting when the DC-link voltage is limited to two levels. The third operation mode allows the voltage application under a minimum active power value demanded from the controller. This mode can be useful when the DC-link is supplied by accumulators and it can prolong its life-cycle.

The third mode for compensating voltage is the main focus of this work. The development of the equation to produce the control reference assuring the minimization of injected active power is as follows. Initially, the equations for active power supplied by the grid and consumed by the load are presented by

$$P_{pcc} = |V_{pcc}| |I| \cos \phi_g \quad (11)$$

$$P_{load} = |V| |I| \cos \phi_l \quad (12)$$

By using the difference between (12) and (11) is possible to

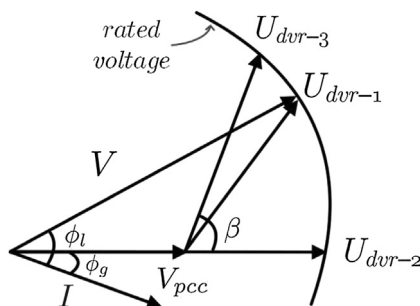


Fig. 4. Voltage vectorial schematic for dropped voltage mitigation.

calculate the active power injected by the controller and it is given by

$$P_{dvr} = |V| |I| \left(\cos \phi_l - \frac{V_{pcc}}{V} \cos \phi_g \right) \quad (13)$$

Eqs. (11)–(13) may be represented in per unit values and the power base is $|V||I|$. In this case, the controller must keep the load voltage in the nominal value ($|V| = 1$). Hence, (13) becomes

$$P_{dvr} = fp_l - |V_{pcc}| \cos \phi_g \quad (14)$$

where $fp_l = \cos \phi_l$. Regarding (14), two possibilities can be reached for the active power injection from the compensator. One possibility is when the injected power is zero. In the second, the power is not zero but it is minimized. This happens due to the intensity of the sag affecting the voltage. Hence, it is necessary to devise a limit of sag which determines whether the first or second possibility is executed by the control system. In the first case, $P_{dvr} = 0$, and the following expression is true

$$0 = fp_l - V_{pcc} \cos \phi_g, \quad (15)$$

and therefore,

$$\cos \phi_g = \left(\frac{fp_l}{|V_{pcc}|} \right) \quad (16)$$

$$\phi_g = \arccos \left(\frac{fp_l}{|V_{pcc}|} \right). \quad (17)$$

Considering $0 < \cos \phi_g \leq 1$, the condition for null injected active power can be reached if

$$|V_{pcc}| \geq fp_l, \quad (18)$$

in other words, the voltage sag in pu value cannot be less than the load power factor.

When (18) is not satisfied, the active power can still be minimized. Hence, the grid supplies a maximum active power, causing current and voltage of the grid to be in phase ($\cos \phi_g = 1$). Hence, the power supplied by the compensator is given by

$$P_{dvr}^{min} = fp_l - |V_{pcc}|. \quad (19)$$

The compensator can absorb power from the grid if P_{dvr}^{min} is negative and this condition must be avoided. From the circuit depicted in Fig. 3, one can write:

$$U_{dvr} = V - V_{pcc} \quad (20)$$

By using phasorial representation (20) is given by:

$$|U_{dvr}| \angle \beta = 1 \angle (\phi_l - \phi_g) - (1 - |V_{pcc}|). \quad (21)$$

Considering the situation where the active power injected is null, the magnitude and the phase of U_{dvr}^0 is represented by

$$\left| U_{dvr}^0 \right| = \sqrt{|V_{pcc}|^2 + 2(1 - |V_{pcc}|)[1 - \cos(\phi_l - \phi_g)]} \quad (22)$$

$$\beta^0 = \arctan \left[\frac{\sin(\phi_l - \phi_g)}{\cos(\phi_l - \phi_g) - (1 - |V_{pcc}|)} \right] \quad (23)$$

Likewise, when the active power injected cannot be null but minimized, U_{dvr}^{min} is represented by

$$\left| U_{dvr}^{min} \right| = \sqrt{|V_{pcc}|^2 + 2(1 - |V_{pcc}|)(1 - \cos \phi_l)} \quad (24)$$

$$\beta^{min} = \arctan \left[\frac{\sin \phi_l}{\cos \phi_l - (1 - |V_{pcc}|)} \right] \quad (25)$$

A RLS algorithm that estimates the parameters from sinusoidal signals [36] is necessary to carry out the proposed method. This

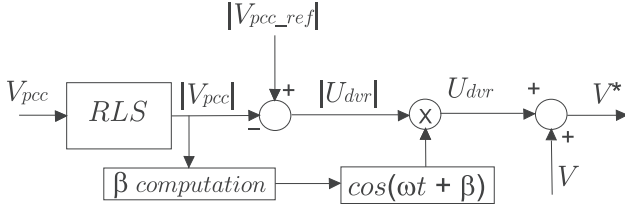


Fig. 5. Recursive least-squares applied to generating set point voltage.

algorithm is discussed in the next section.

4. A recursive Least-Squares algorithm for voltage grid parameters estimation

The scheme presented in Fig. 5 allows the estimation of the voltage reference V^* for the control system is depicted in Fig. 2. One can note that the RLS estimation is applied to furnish the magnitude of the grid voltage. The difference between a given nominal value and this magnitude is applied to the compensating voltage. This result is multiplied by a cosine function with initial phase β which is computed by (23) or (25), depending on whether the injected power is null or minimum. Finally, the injected voltage U_{dvr} subtracts the measured voltage grid to produce V^* .

The estimation of the magnitude and phase of a voltage signal is achieved by the RLS estimator employed in this paper. The RLS is based on a signal model composed by a sum of p sinusoids, with one being the fundamental, and the others being harmonics. This assures the estimator robustness with regards to harmonics. Designating the voltage signals by v_g , the model \hat{v}_g is expressed as

$$\hat{v}_g(n\Delta t) = \hat{v}_g[n] = \sum_m^p V_{Gm} \cos(m\omega_0 n\Delta t + \alpha) \quad (26)$$

where α_m and V_{Gm} being, respectively, the phase and the amplitude of the sinusoid of $m\omega_0$ frequency. Δt is the sample period. The first sinusoid are related to the fundamental phasor.

To adapt (26) for the RLS algorithm, one uses a well-known trigonometrical identity to obtain

$$\hat{v}_g[n] = \sum_{m=1}^p [V_{Gm}^c \cos(m\omega_0 n\Delta t) - V_{Gm}^s \sin(m\omega_0 n\Delta t)], \quad (27)$$

where V_{Gm}^c and V_{Gm}^s are related to the model (26) by using the equations

$$V_{Gm} = \sqrt{(V_{Gm}^c)^2 + (V_{Gm}^s)^2} \quad (28)$$

$$\alpha_m = -\arctan \frac{V_{Gm}^s}{V_{Gm}^c}. \quad (29)$$

Eq. (27) can be written as

$$\hat{v}_g[n] = \phi_n^T \varphi_n, \quad (30)$$

in which ϕ_n is a vector of regressors given by

$$\phi_n = \begin{bmatrix} \cos(\omega_0 n\Delta t) \\ \sin(\omega_0 n\Delta t) \\ \dots \\ \cos(p\omega_0 n\Delta t) \\ \sin(p\omega_0 n\Delta t) \end{bmatrix}, \quad (31)$$

and φ_n is a vector of parameters to be determined and whose elements are given by

$$\varphi_n = [V_{1c} \ V_{1s} \ \dots \ V_{pc} \ V_{ps}]^T. \quad (32)$$

The discordance between v_g and \hat{v}_g at the instant t_n is an error $e[n]$, defined as

$$e[n] = v_g[n] - \hat{v}_g[n]. \quad (33)$$

The RLS algorithm updates the estimative for the parameters according to [37]

$$\hat{\varphi}_{n+1} = \hat{\varphi}_n + \mathbf{K}_{n+1} e[n+1], \quad (34)$$

where \mathbf{K}_{n+1} is a gain defined as

$$\mathbf{K}_n = \mathbf{P}_n \phi_n, \quad (35)$$

and \mathbf{P}_n is the covariance matrix to be updated by the following recursive equation

$$\mathbf{P}_{n+1} = \mathbf{P}_n - \frac{\mathbf{P}_n \phi_n \phi_n^T \mathbf{P}_n}{1 + \phi_n^T \mathbf{P}_n \phi_n}. \quad (36)$$

The covariance matrix is initially adjusted to be diagonal with the elements being high values in comparison with the values of the parameters to be estimated. During the RLS application, as the estimation converges for the true values of the parameters, the \mathbf{P}_n norm is reduced. This means that the algorithm is less adaptable. There are numerous manners to provide adaptability to the algorithm. The one selected here is designated Modified Random Walking (MRW) [38]. In this technique, the covariance matrix is updated according to the following rule

$$\mathbf{P}_{n+1} = \begin{cases} \mathbf{P}_n - \frac{\mathbf{P}_n \phi_n \phi_n^T \mathbf{P}_n}{1 + \phi_n^T \mathbf{P}_n \phi_n} & \text{if } |e[n]| \leq \epsilon \\ \mathbf{P}_n + \mathbf{R} & \text{if } |e[n]| > \epsilon \end{cases} \quad (37)$$

where ϵ is arbitrarily adjusted. It is worth stressing that at each sampling period, the magnitude of the grid voltage is provided by (28).

5. Simulated results

The results depicted in this section have been generated within the *Simulink* environmental. Firstly, two scenarios of faults are here considered to test the capability of the repetitive controller to cope with sag and harmonic distortions.

In the first scenario, the controller deals with the a sagged voltage in one of the phases. The compensated and the sagged voltage are depicted in Fig. 6. The 50% voltage sag starts at 20 ms and ended at 80 ms. The settling time is about 0.2 ms and the overshoot is 5% at the beginning of the sag. From the extinction of the event, the overshoot is 18%. The figure shows that the controller promptly restores the voltage to its nominal parameters. The voltage has a peak during the transient when the voltage sag is finished but it is rapidly suppressed. It can be noticed that the compensated and sagged voltages are in-phase, indicating that the reference to the controller is produced to minimize the compensating voltage amplitude.

The second scenario is shown in Fig. 7 and the voltage is affected by a sag and harmonic distortions simultaneously. The proposed repetitive controller is able to mitigate the voltage sag and the harmonics. The DVR supplies the load with a sinusoidal voltage. The settling time is approximately 0.2 ms, while the overshoot is 4.6% at the beginning and 18% at the end. During the sag the controlled voltage is established to the its rated value and the total harmonic distortion (THD) is 24.63% (grid). The compensated voltage by the controller has the THD of

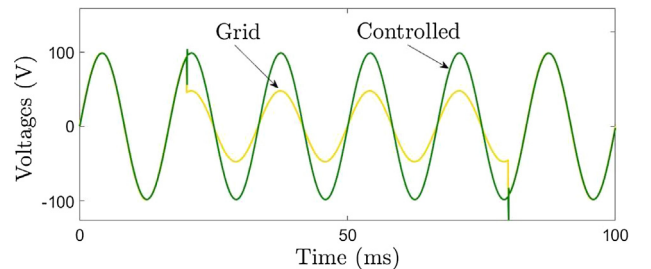


Fig. 6. Voltage sag compensation on the load.

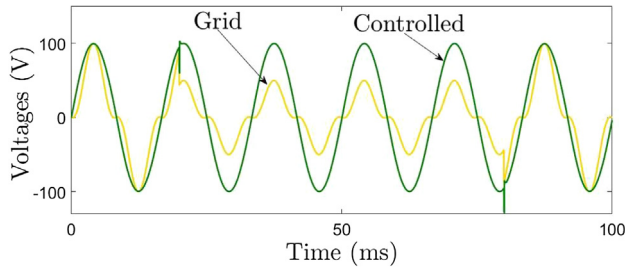
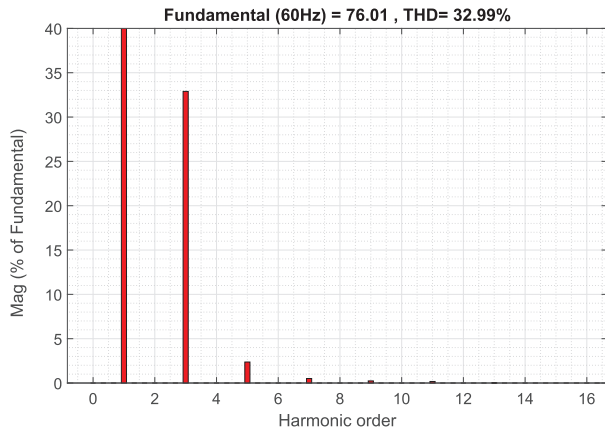
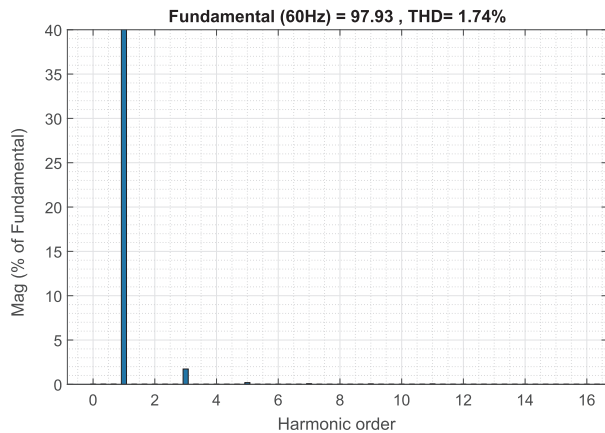


Fig. 7. Voltage sag and distortion compensation on the load.



(a)



(b)

Fig. 8. Total harmonic distortion. (a) Electrical grid. (b) Protected load.

0.97%, illustrating that the DVR compensation is significant. Fig. 8(a) and (b) show the graphs of the magnitudes of the fundamental and the harmonics contained in the distorted grid voltage and the compensated voltage, respectively. It is noticeable that the DVR largely attenuates the harmonics, particularly the third-order one.

A second set of simulated results have been produced illustrating the performance of the DVR when it is protecting a load of power factor of 0.7. In this set, the results for the first simulation are depicted in Fig. 9. Here, the reference for the DVR controller is generated so that the amplitude of the voltage injected by the DVR, U_{DVR} , is minimum. The amplitude of the grid voltage, V_{pcc} , during the sag is about 80% of its nominal value. From the figure, it is evident that the corrected voltage, V , across the load is kept in the expected rated value. The current I is also drawn (in red) in the figure. It is lagged from the V_{pcc} , once the power is not being optimized in this case.

The simulated results to minimum power injection by the DVR are

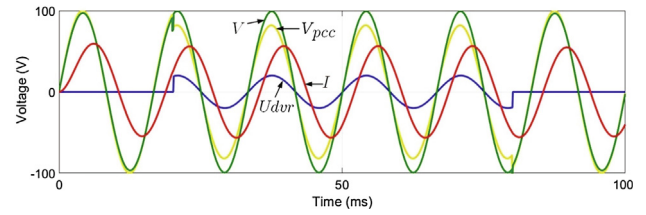


Fig. 9. DVR Compensating results - Minimum voltage injected.

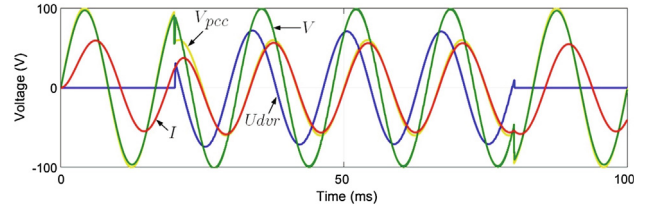


Fig. 10. DVR Compensating results - Minimum power injected.

depicted in Fig. 10. In this case, the sag affecting the voltage imposes the condition $|V_{pcc}| < fp_l$. Hence, the compensating voltage is built with (24) and (25). In the same figure it is possible to observe that the injected voltage is not synchronized with the load voltage nor the pre-sagged grid voltage. The grid voltage is almost in-phase with the current I , assuring that the grid is furnishing as much as possible active power and, consequently minimizing the power provided by the DVR. Thus, this case guarantees the active power supplied by the DVR is minimum. In this case, it is evident that the injected voltage, U_{DVR} is significantly larger when compared to the case shown in Fig. 9.

Another case, yet related to minimizing the output active power from the DVR during compensation, is the situation where the injected power to the grid is zero. In this case, the sag level must be greater than the load power factor, that is, $|V_{pcc}| > fp_l$. Hence, (22) and (23) are used to build the injected voltage. The results for this scenario are shown in Fig. 11. The results show a 90-degree delay between the injected voltage and the load current, indicating null active power from the DVR. The null power injection might be considered a particular case of the minimum power injection strategy. Therefore, the algorithm that controls the voltage compensator must predict this condition to assure that the device reaches its maximum efficiency in terms of energy. The settling time is about 0.05 ms in every waveforms compensations shown in Figs. 9–11.

6. Experimental approach and results

In this section, laboratory experiments have been carried out for corroboration of the simulated results. The power and acquisition-control stages of the experimental setup are shown in the Fig. 12. On the front stage are placed the voltage source inverter (VSI), the power grid, the 1:1 ratio injection transformers, LC PWM filters and RL loads. Accordingly to the simulated results, the load power factor has been fixed in 0.7. The acquisition-control stage is comprised of voltage and current conditioning circuits based on Hall-effect sensors, switched power supplies, and digital signal processor (DSP) from Texas

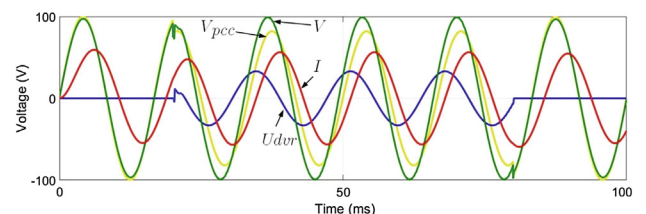


Fig. 11. DVR Compensating results - Zero power injected.

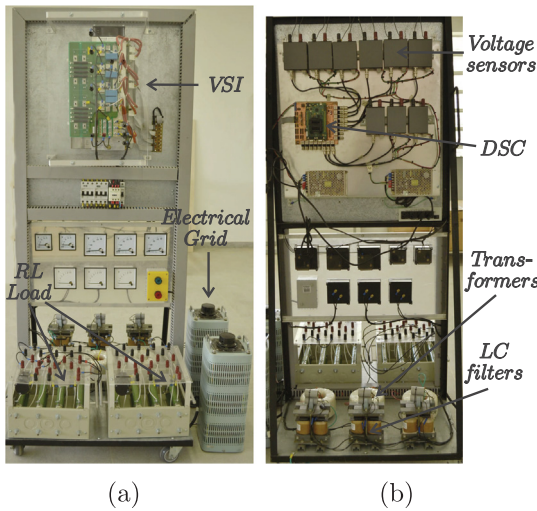


Fig. 12. Laboratory-scale series compensator. (a) Electric grid and power devices. (b) Control and acquisition system.

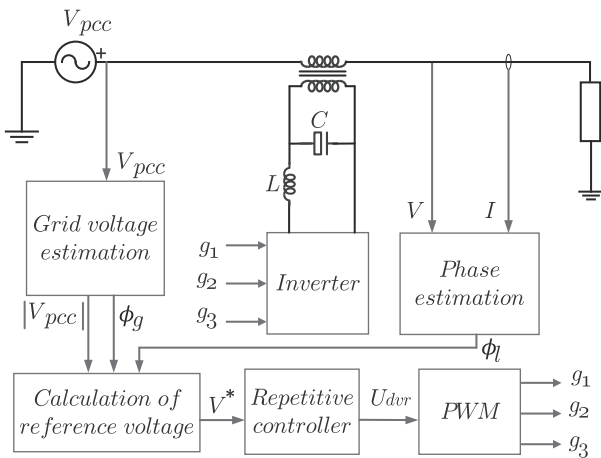


Fig. 13. Schematic diagram of the measuring and control system for load voltage compensation.

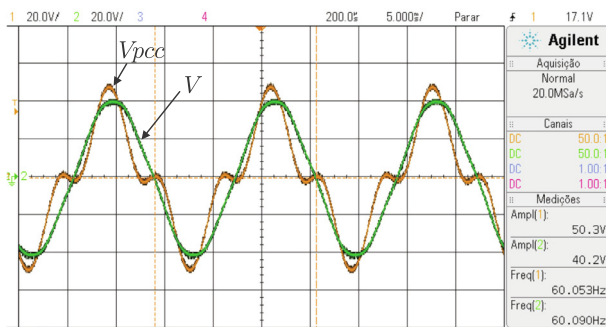


Fig. 14. Experimental results - Harmonic voltage compensation.

Instruments, which has the capability of processing and generating PWM signals that are suitable for this application. The grid faults have been generated with a programmable power source. The repetitive controller is implemented by the trapezoidal integration method. The inverter switching frequency is 10 kHz, which corresponds to the same sampling frequency. The compensating voltages are realized by a digital scalar PWM [39]. For a better understanding of how the measuring system is set together with the control system, a schematic diagram is shown in Fig. 13. To show the effectiveness of the proposed control

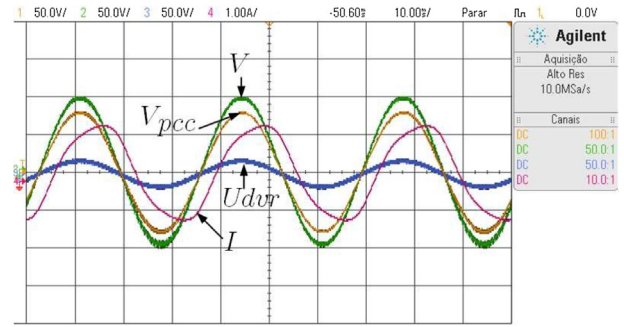


Fig. 15. Experimental results - Minimum voltage injected.

method in mitigating other interferences besides sags, in Fig. 14 is displayed a result on the oscilloscope screen where the DVR regulates harmonic distortions from the grid. This reduction is not the DVR main objective, but it is interesting to explore as extra functionality. It is clear the method greatly reduces the distortions. The harmonic content of the scenario is equal to the simulated case.

Fig. 15 shows the result referring to the approach of the minimum voltage method. As previously described, the injected voltage by the compensator (U_{DVR}) is in phase with the sagged grid (V_{pcc}) ensuring a minimum level of U_{DVR} . Furthermore, as in the simulated case, the sag is 50%. In the same figure, it can still be seen that the current I , which is lagged in relation to the load voltage (inductive current), has a small distortion. This takes place as the current level saturates the load inductors. However, this does not in any way impair the control purposes, since the voltages are corrected by the DVR. The load voltage reaches the desired nominal value for the experimental case, which is 100 V peak.

The results shown in Fig. 16 represent the scenario of minimum power injection by the DVR, since the voltage sag level is about 60%, that is, meeting the request $|V_{pcc}| < \beta p_l$. It can be observed that the current is lagged approximately 90 degrees in relation to the U_{DVR} , which indicates the injected active power is quite low. In addition, the grid voltage and current are near in-phase, which indicates that the grid supplies its maximum power to the load. Despite the merit of the minimum power, the voltage level for the realization of this scenario is almost the double of the previous one. Therefore, the use of one or the other minimum voltage or power criterion is a trade-off of having a minimum voltage level in the compensator DC-link.

The last scenario to be analyzed is the one shown in Fig. 17. The voltage sag level is about 80%, that is, meeting the request $|V_{pcc}| > \beta p_l$. This condition permits zero power injection from the DVR. Here, one can readily notice is a 90 degree delay between the compensating voltage and the load current. Hence the DVR does not inject active power to carry out the voltage compensation. However, the voltage level is higher. The output voltage is restored to its nominal value during the event.

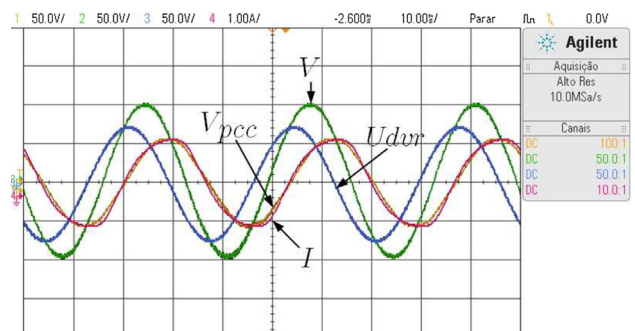


Fig. 16. Experimental results - Minimum power injected.

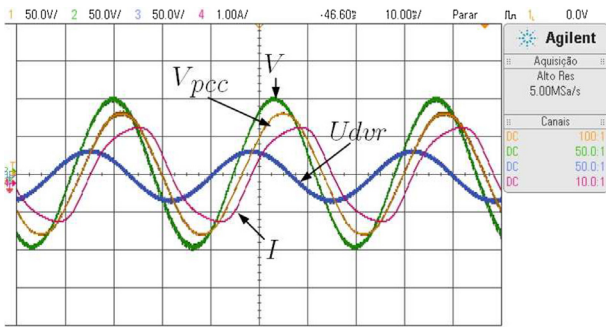


Fig. 17. Experimental results – Zero power injected.

7. Conclusions

This paper has proposed a DVR-based compensation voltage to protect critical loads that relies on the construction of a proper voltage reference to the DVR control system. The tracking of such reference assures that the DVR output power is minimized during a fault occurrence. The reference computation is carried out by using a recursive least square algorithm and the knowledge of the load power factor. Also, the proposed method can be modified to minimize the compensating voltage amplitude. This paper has also proposed a repetitive controller to the DVR able which is stable and robust to harmonic distortions. This feature allows the proposed compensation method to cope with harmonics and sags simultaneously. Also, the proposed method can be promptly applied to single-phase systems because it is applied separately in each phase of the three-phase grid and, therefore, does not require the use of sequence estimation procedures, unlike schemes based on synchronous reference frames controllers. An experimental setup has been mounted to verify all scenarios that have been computationally simulated. The results ratifies the proposed controller and demonstrate its efficacy.

Declaration of Competing Interest

The authors declare that they have no known competing financial interests or personal relationships that could have appeared to influence the work reported in this paper.

Acknowledgment

The authors would like to thank the Brazilian Research Councils Capes through the Process PVEX-88881.170495/2018-01, CNPq Process 437435/2018-0, CNPq n°430779/2018-6 and CNPq 405757/2018-2.

References

- [1] Swain S, Ray P, Mohanty K. Improvement of power quality using a robust hybrid series active power filter. *IEEE Trans Power Electron* 2017;32(5):3490–8.
- [2] Park CH, Jang G. Systematic method to identify an area of vulnerability to voltage sags. *IEEE Trans Power Del* 2017;32(3):1583–91.
- [3] Li P, Xie L, Han J, Pang S, Li P. A new voltage compensation philosophy for dynamic voltage restorer to mitigate voltage sags using three-phase voltage ellipse parameters. *IEEE Trans Power Electron* 2018;33(2):1554–66.
- [4] Krishnamurthy V, Kwasinski A. Effects of power electronics, energy storage, power distribution architecture, and lifeline dependencies on microgrid resiliency during extreme events. *IEEE J Emerg Sel Topics Power Electron* 2016;4(4):1310–26.
- [5] Varela J, Hatzigiorgianni N, Puglisi LJ, Bissel G, Abart A, Rossi M, et al. The best of green grid practices: A distribution network's contribution to resiliency. *IEEE Power Energy Mag* 2016;13(3):81–9.
- [6] Manshadi SD, Khodayar ME. Resilient operation of multiple energy carrier microgrids. *IEEE Trans Smart Grid* 2015;6(5):2283–92.
- [7] Hussein AA, Ali MH. Comparison among series compensators for transient stability

- enhancement of doubly fed induction generator based variable speed wind turbines. *IET Renew Power Gen* 2016;10(1):116–26.
- [8] Shahabadi M, Iman-Eini H. Improving the performance of a cascaded H-bridge-based interline dynamic voltage restorer. *IEEE Trans Power Del* 2016;31(3):1160–7.
- [9] Inci M, Bayindir KC, Tumay M. The performance improvement of dynamic voltage restorer based on bidirectional dc-dc converter. *Electr Eng* 2017;99(1):285–300.
- [10] Jothibasu S, Mishra M. An improved direct AC-AC converter for voltage sag mitigation. *IEEE Trans Ind Electron* 2015;62(1):21–9.
- [11] Hao H, Yonghai X. Control strategy of PV inverter under unbalanced grid voltage sag. In: *IEEE Energy Conv. Cong. & Expo., ECCE*, vol. 1; 2014. p. 1029–34.
- [12] He L, Zhang K, Xiong J, Fan S. A repetitive control scheme for harmonic suppression of circulating current in modular multilevel converters. *IEEE Trans Power Electron* 2015;30(1):471–81.
- [13] Chen D, Zhang J, Qian Z. An improved repetitive control scheme for grid-connected inverter with frequency-adaptive capability. *IEEE Trans Ind Electron* 2013;60(2):814–23.
- [14] Li YW, Vilathgamuwa DM, Blaabjerg F, Loh P. A robust control scheme for medium-voltage-level dvr implementation. *IEEE Trans Ind Electron* 2007;54(4):2249–61.
- [15] Keerthipati S, Nallamekala K. Blackupsc svpwm controlled multi-level inverter topology for multiple pole-pair induction motor drive for minimizing torque ripple. *IET Power Electron* 2016;9(6):1306–14.
- [16] Naidu SR, Fernandes DA. Dynamic voltage restorer based on a four-leg voltage source converter. *IET Gen Trans Distrib* 2009;3(5):437–47.
- [17] Nielsen JG, Blaabjerg F. A detailed comparison of system topologies for dynamic voltage restorers. *IEEE Trans Ind Appl* 2005;41(5):1272–80.
- [18] Ye J, Gooi HB, Wang B, Li Y, Liu Y. Elliptical restoration based single-phase dynamic voltage restorer for source power factor correction. *Electric Power Syst Res* 2019;166:199–209.
- [19] Li Y, Blaabjerg F, Vilathgamuwa D, Loh P. Design and comparison of high performance stationary-frame controllers for DVR implementation. *IEEE Trans Power Electron* 2007;22(2):602–12.
- [20] Tu C, Guo Q, Jiang F, Shuai Z, He X. Analysis and control of bridge-type fault current limiter integrated with the dynamic voltage restorer. *Int J Electr Power Energy Syst* 2018;95:315–26.
- [21] Omar AI, Aleem SHEA, El-Zahab EEA, Algablawy M, Ali ZM. An improved approach for robust control of dynamic voltage restorer and power quality enhancement using grasshopper optimization algorithm. *ISA Trans* 2019:1–20 available online.
- [22] Gamboa P, Silva JF, Pinto SF, Margato E. Input-output linearization and PI controllers for AC-AC matrix converter. *Electric Power Syst Res* 2019;169:214–28.
- [23] Arablouei R, Dog'any K, Werner S. Recursive total least-squares algorithm based on inverse power method and dichotomous coordinate-descent iterations. *IEEE Trans Signal Process* 2015;63(8):1941–9.
- [24] Engel Y, Mannor S, Meir R. The kernel recursive least-squares algorithm. *IEEE Trans Signal Process* 2004;52(8):2275–85.
- [25] Meral ME, Celik D. A comprehensive survey on control strategies of distributed generation power systems under normal and abnormal conditions. *Ann Rev Control* 2018:1–21 available online.
- [26] Zhang K, Kang Y, Xiong J, Chen J. Direct repetitive control of SPWM inverter for UPS purpose. *IEEE Trans Power Electron* 2003;18(3):1310–26.
- [27] Inci M, Bayindir KC, Tumay M. Improved synchronous reference frame based controller method for multifunctional compensation. *Electric Power Syst Res* 2016;141(1):500–9.
- [28] Twining E, Holmes DG. Grid current regulation of a three-phase voltage source inverter with an LCL input filter. *IEEE Trans Power Electron* 2003;18(3):888–95.
- [29] Teodorescu R, Blaabjerg F, Liserre M, Loh PC. Proportional-resonant controllers and filters for grid-connected voltage-source converters. *IEEE Proc-Electr Power Appl* 2006;153(5):750–62.
- [30] Meral ME, Celik D. Comparison of SRF/PI and STRF/PR-based power controllers for grid-tied distributed generation systems. *Electr Eng* 2018;100(2):633–43.
- [31] Rohouma W, Zanchetta P, Wheeler PW, Empringham L. A four-leg matrix converter ground power unit with repetitive voltage control. *IEEE Trans Ind Electron* 2015;62(4):2032–40.
- [32] Nie X, Qiao H, Zhang B, Huang X. A nonlocal tv-based variational method for polars data speckle reduction. *IEEE Trans Image Process* 2016;25(6):2032–40.
- [33] Celik D, Meral ME. A flexible control strategy with overcurrent limitation in distributed generation systems. *Electrical Power Energy Syst* 2019:456–71.
- [34] Hara S, Yamamoto Y, Omata T, Nakano M. Repetitive control system: A new type servo system for periodic exogenous signals. *IEEE Trans Autom Control* 1988;33(7):659–68.
- [35] Sanchez P, Acha E, Calderon J, Feliu V, Cerrada A. A versatile control scheme for a dynamic voltage restorer for power quality improvement. *IEEE Trans Power Del* 2009;24(1):277–84.
- [36] Fernandes DA, Costa FF, Vitorino MA. A method for averting saturation from series transformers of dynamic voltage restorers. *IEEE Trans Power Del* 2014;29(5):2239–47.
- [37] Ljung L. System identification: theory for the user. 2nd ed. Prentice Hall PTR; 1999.
- [38] Costa FF, Formiga DA, Ferreira RR, Sousa T, Costa FB. A recursive least-squares aided by pre-filtering for phasor-estimation in distance protection. *Powertech, IEEE-PES, Grenoble-France*. 2013.
- [39] Fernandes DA, Costa FF, Jr ECS. Digital-scalar PWM approaches applied to four-leg voltage-source inverters. *IEEE Trans Ind Electron* 2013;60(5):2022–30.